

**AN AIRBORNE SPECTRAL ALBEDOMETER
WITH ACTIVE HORIZONTAL STABILIZATION**

Manfred Wendisch¹, Dörthe Müller¹, Dieter Schell², and Jost Heintzenberg¹

¹Institute for Tropospheric Research, Leipzig, 04318, Germany

²*enviscope* GmbH, Frankfurt/M., 60489, Germany

Revised version of a MANUSCRIPT

submitted to *J. Atmos. Oceanic Technol.*

April 2001

Corresponding author address: Manfred Wendisch, Institut für
Troposphärenforschung e.V. (IfT), Permoserstr. 15, 04318 Leipzig, Germany.
E-mail: wendisch@tropos.de

ABSTRACT:

We have developed an airborne albedometer including a low-cost, precise and fast sensor head horizontal stabilization system to measure spectral down- and upward irradiances between 400 and 1000 nm wavelength. It is installed on a small research aircraft (type Partenavia P68-B), but it can easily be mounted on other aircraft as well. The stabilization unit keeps the two radiation sensor heads (up- and downward looking) of the albedometer in a horizontal position during the flight with an accuracy of better than $\pm 0.2^\circ$ over a range of pitch and roll angles of $\pm 6^\circ$. The system works properly for angular velocities up to 3°s^{-1} with a response time of the horizontal adjustment of 43 ms. Thus it can be applied even under turbulent atmospheric conditions. The limitations of the stabilization have been determined by laboratory and in-flight performance tests. As a result we find that the new horizontal stabilization system assures that misalignment-related uncertainties of the measured irradiances are less than 1% for solar zenith angles up to 70° . This does not include uncertainties due to deviations from the ideal cosine response of the optical inlet system and measurement errors resulting from absolute calibration problems. An example of downward spectral irradiances measured under cloudless conditions above and within a distinct boundary layer with enhanced aerosol particle concentrations shows the potential of the new instrument for improved radiative budget measurements in the atmosphere.

1. INTRODUCTION

The Earth's climate is mostly driven by the incoming solar radiation, which is characterized by so-called irradiances. This energetic quantity is defined as the radiative energy incident per second upon a horizontal unit area. To study the transfer of incoming solar radiation through the atmosphere, airborne irradiance measurements at different altitudes are required. Measurements of irradiances from airborne platforms are afflicted with several serious problems, which magnify if e.g. optical cloud properties are derived from the data. Part of the confusion in the literature about how well measured and calculated cloud absorption agree (so-called 'enhanced cloud absorption', see Stephens 1996) results from such unresolved irradiance measurement uncertainties.

Numerous experimental problems have been mentioned in the measurements of irradiances. Kiedron et al. (1999) found that even NIST (National Institute of Standards and Technology) standard lamps used for absolute spectral irradiance calibrations may disagree with each other beyond their stated uncertainty. Furthermore, the separation between diffuse and direct portion of the irradiances is not easy to obtain (Foot et al., 1985) especially for airborne operation (Forgan, 1996; Boers et al., 1998). On the other hand, the diffuse to direct ratio has to be known in order to correct the irradiance data for non-ideal cosine response of the used light collectors (Feister et al., 1997; Oppitz and Heering, 1998; Bais et al., 1998; Landelius and Joseffson, 2000). Furthermore, there are re-radiative thermal offsets in the instruments (Beaubien et al., 1998; Bush et al., 2000), which need to be considered (Halthore and Schwartz, 2000). These offsets appear if the instruments are operated in environments with strongly varying temperature.

Beside these issues, there are two further crucial problems associated with airborne irradiance measurements, which are specially addressed in this paper: (i) uncertainties related to deviations of the sensor detection plane from the Earth's horizon, and (ii) spectral resolution of the measurements.

By definition, irradiances refer to the horizontal unit plane of the Earth-fixed coordinate system. As the irradiance instruments are mostly fixed on the aircraft fuselage, pitch and roll movements during the flight cause deviations of the sensor detection plane from the horizontal reference plane of the Earth-fixed coordinate frame. Additionally, there are unavoidable deviations of the sensor detection plane with respect to the horizontal plane of the aircraft-fixed coordinate frame due to installation requirements. Until now, these so-called sensor misalignment problems (i.e. sensor horizontal plane deviations from the ideal horizon) are considered in two ways: (1) data are rejected if certain pitch and roll angle limits are exceeded, or (2) software post-flight correction procedures are applied (Saunders et al., 1992; Asano and Shiobara, 1989; Bannehr and Glover, 1991; Bannehr and Schwiesow, 1993; Boers et al., 1998). These post-flight correction techniques account for geometric deviations. They cannot remove physical artifacts caused by the tilted sensor, such as unknown angular distribution of the diffuse radiation or mixing of e.g. diffuse upward irradiances (erroneously sampled by the tilted upward looking sensor) with downward irradiances and vice versa. Therefore, these correction procedures provide good results in clear atmospheres, i.e. where the direct beam of the sun dominates. In atmospheres with heavy aerosol loads or in broken cloud fields (i.e. much isotropic diffuse radiation) these numerical correction techniques are not satisfying.

The second problem arises from the missing spectral resolution of most of the airborne irradiance sensors. Commonly, pyranometers (most of them are manufactured by The Eppley Laboratory, Inc., Newport, RI, USA) are used to measure broadband up- and downward irradiances integrated over the solar spectral range (wavelengths between about 0.3 and 3 μm) from aircraft (e.g. Hobbs, 1999) or balloons (Hagan et al., 1998). To achieve some coarse spectral separation, it is popular to use two Eppley pyranometers simultaneously, one with a clear dome with a transmission between 0.3 and 3 μm and another one with a red dome transparent between 0.7 and 3 μm . Subsequently the solar spectral range is split into its visible ($\approx 0.3\text{-}0.7$ μm) and infrared ($\approx 0.7\text{-}3$ μm) portions (Hignett, 1987; Saunders et al., 1992; Taylor, 1994; Taylor and McHaffie, 1994; Hayasaka et al., 1995; Taylor et al., 1996; Hignett et al., 1999; Russell et al., 1999; Taylor and Ackerman, 1999). There are some airborne irradiance data available with slightly better spectral resolution (up to about ten wavelengths) using interference filters for the wavelength separation and silicon or germanium photodiodes as detector for the wavelength region below and above 1 μm respectively (Asano et al., 1995a; Asano et al., 1995b; Valero et al., 1996). Irradiance measurements of higher spectral resolution are mostly restricted to ground-based instruments (Harrison et al., 1999; Meywerk and Ramanathan, 1999; Michalsky et al., 1999; Wendisch et al., 2001) and to the ultraviolet or near-infrared spectral range (e.g. Ramaswamy and Freidenreich, 1998; Sicard et al., 1998). Spectral actinic irradiances, which are related to the surface of a unit sphere instead of a horizontal unit area like in the case of common irradiances, are also mostly measured at the ground (Hofzumahaus et al., 1999). A new airborne system

for spectral actinic irradiance measurements is recently reported by Shetter and Müller (1999).

To overcome the two problems of horizontal sensor misalignment and missing spectral resolution of the irradiance measurements we have developed an airborne spectral albedometer system for measurements of spectral (400-1000 nm) up- and downward irradiances from an aircraft, which is equipped with an in-flight active horizontal stabilization system. In Section 2 we motivate the development of the horizontal stabilization by quantifying the misalignment-related uncertainties of irradiance measurements and of derived optical properties of atmospheric layers (e.g. aerosol or cloud layers, whole atmosphere). The technical details of the horizontal stabilization system are given in Section 3. This includes laboratory tests of the horizontal stabilization system using both artificially generated and real aircraft attitude data. Some results of in-flight performance tests of the horizontal stabilization system and examples of downward irradiance measurements under cloudless conditions above and within a pronounced boundary layer are presented in Section 4. The conclusions of the paper and a short outlook are given in Section 5.

2. UNCERTAINTIES DUE TO HORIZONTAL MISALIGNMENT

In order to quantify the uncertainties associated with the sensor horizontal misalignment we have done some simple calculations. We define the dimensionless error factor ψ of the radiation quantity ζ as the ratio of the 'biased' (due to misalignment) to the 'unbiased' (assuming perfect horizontal alignment) value of the respective radiation quantity ζ :

$$\psi_{\zeta} = \zeta_{\text{biased}} / \zeta_{\text{unbiased}} \quad (1).$$

As an example we obtain the error factor of the irradiance F (i.e. $\zeta = F$) depending on the zenith angle θ of the incident radiation and the horizontal misalignment $\Delta\theta$ by:

$$\psi_F(\theta, \Delta\theta) = F_{\text{biased}}/F_{\text{unbiased}} = \cos(\theta + \Delta\theta)/\cos\theta \quad (2).$$

Furthermore, we define the percentage deviation Φ_ζ [%] of the radiation quantity ζ due to horizontal misalignment by:

$$\Phi_\zeta = (\psi_\zeta - 1) \cdot 100\% \quad (3).$$

To evaluate the impact of the horizontal misalignment $\Delta\theta$ on the measurements of irradiance and of several optical properties of atmospheric layers (like aerosol or cloud layers, or the whole atmosphere), derived from these irradiance measurements, we have calculated their percentage deviations Φ_ζ as a function of the zenith angle θ and the misalignment $\Delta\theta$. The optical properties investigated are the layer's top albedo r , the layer reflectance R , the layer transmittance T , the irradiance absorbed in the layer F_a , and the layer absorptance A . These optical properties are defined as follows:

$$r = F\uparrow_{\text{TOP}}/F\downarrow_{\text{TOP}} \quad (4),$$

$$R = (F\uparrow_{\text{TOP}} - F\uparrow_{\text{BASE}})/F\downarrow_{\text{TOP}} \quad (5),$$

$$T = F\downarrow_{\text{BASE}}/F\downarrow_{\text{TOP}} \quad (6),$$

$$F_a = (F\downarrow_{\text{TOP}} - F\uparrow_{\text{TOP}}) - (F\downarrow_{\text{BASE}} - F\uparrow_{\text{BASE}}) \quad (7),$$

$$A = F_a/F\downarrow_{\text{TOP}} \quad (8),$$

with $F\uparrow_{\text{TOP}}$ and $F\downarrow_{\text{TOP}}$ the up- and downward irradiances at the top of the layer and $F\uparrow_{\text{BASE}}$ and $F\downarrow_{\text{BASE}}$ the respective up- and downward irradiances at the layer base.

In the following calculations only the term $F\downarrow_{\text{TOP}}$ was truncated with the horizontal misalignment $\Delta\theta$. Especially in the case of a cloud layer this

assumption is well justified. Above the cloud layer the downward radiation consists of the dominant direct portion (highly sensitive to $\Delta\theta$) and the secondary diffuse part of solar radiation (much less sensitive to $\Delta\theta$). Within and below the cloud layer and for all upward irradiance components only diffuse radiation with less misalignment sensitivity is present. In this way the above assumption means that mostly direct solar radiation is afflicted with the horizontal misalignment. Consequently the zenith angle of the incident radiation is identical to the solar zenith angle in our calculations.

Results of the simulations are presented in Figures 1 and 2 and in Tables 1 and 2. Figure 1 shows the percentage deviation of irradiances Φ_F calculated from Eqs. 2 and 3. It becomes obvious, that small horizontal misalignments $\Delta\theta$ can drastically influence the measured irradiances. As expected, these deviations increase for larger solar zenith angles θ . If an accuracy of only 4-5% of the irradiance measurements is desired, then (for $\theta = 70^\circ$) a horizontal alignment of the irradiance sensor of about 1° has to be assured. This is impossible during normal flight operations. Even if the pilot can manage to maintain the aircraft attitude within a $\pm 1^\circ$ range around the horizon, there are inherent mounting misalignments of the fixed radiation sensors with respect to the aircraft-fixed coordinate frame, which usually are in the range of $\pm 1^\circ$. Thus, it seems to be hopeless to assure a 4-5% accuracy of measured irradiances with an irradiance sensor fixed at the aircraft fuselage.

The uncertainties of the measured irradiances transfer into percentage deviations Φ_ζ of the layer optical properties r , R , and T , which are only slightly larger than those of F , though with opposite sign. Therefore, we do not show plots of the percentage deviations for these three layer optical quantities.

Please note that due to the definitions in Eqs. 4-6, it holds that these percentage deviations are identical, i.e. $\Phi_r = \Phi_R = \Phi_T$.

In Figure 2 the percentage deviations of the layer absorptance A due to horizontal misalignments $\Delta\theta$ are plotted. Their magnitude is similar to the respective values for the layer-absorbed irradiances F_a , therefore only results for Φ_A are presented. Because the cloud-absorbed irradiance F_a is no relative quantity (like r , R , and T), we have to use actual irradiance measurements to calculate Φ_{F_a} and Φ_A . For this purpose we have taken measured irradiance data given in Table 6 of Wendisch and Keil (1999). For the calculations in Figure 2 and Table 1 and 2 the special case '09 December upward' is used here ($F_{\uparrow\text{TOP}} = 234 \text{ W m}^{-2}$, $F_{\downarrow\text{TOP}} = 287 \text{ W m}^{-2}$, $F_{\uparrow\text{BASE}} = 1 \text{ W m}^{-2}$, $F_{\downarrow\text{BASE}} = 14 \text{ W m}^{-2}$). Calculations with the other examples given by Wendisch and Keil (1999) revealed even stronger effects. Irradiances absorbed within an atmospheric layer (e.g. a cloud) result from a small residuum of net irradiances (difference between down- and upward irradiances) measured at the top and the bottom of the layer (see Eq. 7). Therefore it is no surprise, that uncertainties in layer top downward irradiances (here due to horizontal misalignments $\Delta\theta$) cause drastic effects in both the irradiances absorbed within the layer and layer absorptance. The magnitude of these errors is large and raises serious doubts about the reliability of measured cloud absorptance values reported in literature, which were always based on radiation sensors fixed at the aircraft fuselage without horizontal adjustment.

Some additional results of the uncertainty propagation calculations are given in Tables 1 and 2. It is important to understand how critically sensitive the irradiances and the investigated layer properties are with respect to relatively small horizontal misalignments $\Delta\theta$ of 0.2° and 1° . For example, the assumption

of a $\Delta\theta = 1^\circ$ yields an uncertainty of F_a and A of about 30-35% for $\theta = 70^\circ$. For $\theta > 40^\circ$ the uncertainties of F_a caused by a horizontal misalignment of $\Delta\theta = 1^\circ$ are always above 10%.

From these results it can be concluded that an accuracy of the horizontal stabilization of $\pm 0.2^\circ$ is needed in order to keep the misalignment-related uncertainty of the measured irradiances below 1% for solar zenith angles up to 70° . We have realized this demand by developing an airborne horizontal stabilization system for a new spectral albedometer.

3. TECHNICAL SETUP

The technical setup of the albedometer is illustrated in Figure 3. The instrument consists of two major components: A horizontal stabilization system (Section 3.1.) and an irradiance measurement unit including two separate radiation sensors (Section 3.2.). The optical inlets (cosine response collectors) of both sensors are mounted at the top and the bottom of the aircraft and are actively stabilized in a horizontal position with respect to the Earth-fixed coordinate system during the flight.

3.1. Horizontal Stabilization System

We have developed a low-cost, precise and fast horizontal stabilization technique for both the up- and downward looking part of the albedometer. The technical challenge is to precisely measure the roll and pitch angles on an accelerated platform (in our case an aircraft) and to use these measurements to compensate the aircraft attitude changes in real-time with a desired final adjustment accuracy better than $\pm 0.2^\circ$.

3.1.1. System Setup

The horizontal stabilization involves two parts (Figure 3): (i) An accurate aircraft roll and pitch angle measurement unit, and (ii) the active horizontal adjustment system.

(i) Roll and Pitch Angle Measurements: Usual inclination sensors measure the tilt of a coordinate system with respect to the Earth's gravity vector. On accelerated platforms like an aircraft this technique does not work because the sensor cannot distinguish between the Earth's gravity and the acceleration vector of the moved platform. In this case a so-called artificial horizon (AHZ) has to be applied. The artificial horizon used here was developed by iMAR GmbH (St. Ingbert, Germany) and consists of two components: (a) three linear servo-acceleration sensors (ACS), which deliver the aircraft velocity and position with respect to the inertial Earth-fixed coordinate system by integration of the lateral acceleration measurements, and (b) three fiber optical gyros, which measure angular rates also with respect to the inertial Earth-fixed frame. From these data the aircraft attitude angles (i.e. roll and pitch) are derived. However, the measurements of the acceleration sensors as well as of the fiber optical gyros are affected by temporal drifts due to sensor errors and electronic noise. These drifts are compensated by using supporting information from a global positioning system (GPS). We use a BeeLine GPS (manufactured by NovAtel Inc., Calgary, Alberta, Canada), which includes a dual antenna configuration to measure the heading and pitch angle in addition to the position and velocity data usually obtained by a single GPS antenna setup. The combined artificial horizon and GPS data are processed and the resulting accurate position and attitude data are stored on a data acquisition system (DAS1). We have also thought about using a four antenna GPS system (e.g.

the TANS Vector GPS Attitude system manufactured by Trimble, Austin, Texas, USA). However, in contrast to our experimental setup, the Trimble system does not deliver the accuracy needed for real-time active horizontal adjustment of the sensors also due to the limited temporal response of the GPS data.

(ii) Active Horizontal Adjustment: The processor unit transfers analog output signals of the roll and pitch angles to a personal computer (PC1), which is equipped with a FlexMotion plug in card (manufactured by National Instruments Corp., Austin, Texas, USA). This card drives (after amplification) two separate 2-dimensional tilt stages (2DTS), which are connected with the cardinally mounted optical inlet (OI) systems of the radiation sensors. Each of the two separate 2-dimensional tilt stages consists of two servo motors, which realize the horizontal adjustment of the albedometer optical inlets. A maximum range of adjustment of $\pm 6^\circ$ is possible. Additionally, the measured attitude data from the combined artificial horizon/GPS system and the signals to drive the server motor are stored on a second data acquisition system (DAS2).

3.1.2. Laboratory Tests

In order to evaluate the general performance of the horizontal stabilization system we have carried out several laboratory tests under static conditions (i.e. no external accelerations acting on the measurement system). These tests have to be complemented by in-flight performance tests (Section 4.1.) in order to confirm the stabilization performance under dynamic conditions, i.e. including external accelerations. We have tested (i) the zero-point stability, (ii)

absolute calibration and linearity of the system and (iii) the reproducibility of pre-defined, simulated albedometer optical inlet movements.

(i) Zero-Point Stability: To test the zero-point stability of the roll and pitch angle measurements from the artificial horizon (supported by the GPS), first both angles were adjusted to 0° and then the system was observed over a 30 minutes time period. Within this period both angles, recorded by the data acquisition system (DAS1) with a 10 Hz sampling rate, varied within a range of $\pm 0.025^\circ$ with a standard deviation of $\pm 0.010^\circ$. However, already after 10 s disabling the drift compensation function, the measured (by the artificial horizon) roll and pitch angles started to drift (in the static case this is only the optical gyro drift) out of the $\pm 0.025^\circ$ range. Some dependence of this drift behavior from the artificial horizon sensor temperature was observed, but not further evaluated.

(ii) Absolute Calibration and Linearity: In order to evaluate the absolute calibration and the linearity of the artificial horizon, a laser and the artificial horizon were fixed at the top of one of the 2-dimensional tilt stages. Then this 2-dimensional tilt stage was stepwise tilted using its control software. Afterwards the roll and pitch angle data from the artificial horizon (recorded by the data acquisition system) were compared with the angles, geometrically derived from the fixed distance between the rotation point of a laser and its beam projection point. The respective regression curve showed an excellent linearity between $\pm 8^\circ$ with a regression slope of 0.99 (coefficient of correlation of 0.99999). The standard deviation of the single data points from the regression line was in the range of $\pm 0.015^\circ$.

(iii) Reproducibility of Simulated Albedometer Sensor Movements: Some further experiments were done with the fixed artificial horizon system at the top

of one of the 2-dimensional tilt stages. In this setup the radiation sensor is replaced by the artificial horizon. Then, instead of using the measured angles (from the artificial horizon/GPS system), as done in usual operation, a function generator was taken to produce pre-defined roll and pitch angle changes to drive the 2-dimensional tilt stage. The function generator was programmed to simulate two types of movements: (a) artificial rectangle- or sinus-type of movements and (b) real aircraft movements recorded during actual aircraft measurements. Comparing the measured (by the GPS-supported artificial horizon fixed at the top of the 2-dimensional tilt stage) and the generated roll and pitch angles allows a quantitative evaluation of the horizontal stabilization system performance under static conditions.

(iii a) First a rectangular pattern with a duration of 10 s and a voltage corresponding to an amplitude of $\pm 3.6^\circ$ was simulated by the function generator. From this experiment a maximum possible angular velocity of 6°s^{-1} and a response time of 43 ms were determined. Similar experiments with a sinus-type pattern of temporal angle changes have shown that the deviations between the measured and the generated angles are in the range of $\pm 0.2^\circ$ for angle velocities of up to 5°s^{-1} .

(iii b) In a second step, roll and pitch angle data previously recorded during real flights were used to drive the 2-dimensional tilt stage by the function generator. Two examples were investigated in detail: A first case was characterized by nearly calm atmospheric conditions and a constant flight altitude of about 3.300 m. The second case was a descending flight pattern from about 1.700 m altitude to 330 m in more turbulent atmospheric conditions. The flights were performed on 16 November 1999 as part of a campaign conducted in Germany (see also Section 4). Here we show only data from the second case, with much

stronger atmospheric turbulence. The given (by the function generator) real flight data and the measured (by the GPS-supported artificial horizon system) attitude angles are shown in Figure 4 (roll angle) and Figure 5 (pitch angle). The lower panels in both figures display the 'Given' (with 10 Hz resolution) and 'Measured' (with 1 Hz resolution only, to make the data points discernable) angles. The upper panels present the respective absolute differences between given and measured roll and pitch angles. Near the end of the time period (after about 210 s) the aircraft descended into the more turbulent planetary boundary layer (PBL) with a distinct temperature inversion at its top. This becomes obvious by enhanced fluctuations of the given and measured angles, as well as in larger absolute differences. However, the horizontal stabilization system worked properly in these turbulent conditions with absolute differences mostly less than 0.1° in both roll and pitch angle. On average a difference of $\pm 0.045^\circ$ for the roll and of $\pm 0.050^\circ$ for the pitch angle was observed. For the first measurement case observed under calm conditions, the absolute differences between given and measured angles were $\pm 0.034^\circ$ for the roll and $\pm 0.050^\circ$ for the pitch axis.

An overall maximum uncertainty of the horizontal stabilization system under static conditions of $\pm 0.2^\circ$ for angular velocities up to 3°s^{-1} is estimated from the laboratory tests.

3.2. Irradiance Measurement Unit

The configuration of the irradiance measurement unit (manufactured by Meteorologie Consult GmbH, Glashütten, Germany) is shown in the lower part of Figure 3. There are two components for separate measurements of the spectral down- and upward irradiances (F_\downarrow and F_\uparrow), which are mounted at the

top and the bottom of the aircraft fuselage. Each of the two components is quite similar to the ground-based instrument described by Wendisch et al. (2001). Two separate optical inlet systems with a cosine response collect the light and yield a measurement signal which is proportional to F_{\downarrow} and F_{\uparrow} , respectively. The two optical inlet systems consist of cosine diffuser domes manufactured from quartz glass. The uncertainty of the cosine-weighting (so-called cosine error) of the entrance optics was determined in the laboratory in order to correct measurement errors caused by non-ideal cosine response of the optical inlet systems. For the upward looking sensor (which measures the most angular-sensitive downward irradiances) an average deviation from the ideal cosine response of the sensor head of 3% (maximum deviation of 5.5% for $\theta = 65^\circ$) was determined, which is pretty low compared to other cosine response collectors. Each of the two optical inlet systems is connected via fiber optics with a multi-channel spectrometer (MCS) module (manufactured by Zeiss GmbH, Jena, Germany), consisting of a fixed grating for wavelength splitting and a 1024 pixel diode array (designed to cover the visible and near-infrared spectral range between about 400 and 1000 nm wavelength) for simultaneous detection of the spectral radiation. The measured signals are transferred to a personal computer (PC2) for raw data acquisition and analysis. The spectrometer has been calibrated in absolute irradiance units ($\text{W m}^{-2} \text{nm}^{-1}$) using a 200 W tungsten halogen lamp (manufactured by OMTec GmbH, Teltow, Germany, lamp no. 031), that is traceable to an absolute level (PTB-SL 144) maintained at the Physikalisch Technische Bundesanstalt (PTB, German Metrology Institute) with an absolute accuracy of $\pm 3\%$ in the visible (400-750 nm) and $\pm 5\%$ in the near-infrared (750-1200 nm) spectral region. The absolute wavelength accuracy is given by the manufacturer to be less than 0.3 nm. The

wavelength calibration of the multi-channel spectrometer module has been checked using mercury lamps. Furthermore, we have determined the FWHM (Full-Width Half-Maximum) of the used spectrometers between 1.8 and 3.5 nm depending on the wavelength. For these measurements we have used several gas lamps (Hg, Kr, Ne, Xe, Ar) with distinct spectral peaks. For the wavelength range covered by our spectrometers the stray light contribution is negligible (< 0.1%).

The two optical inlet systems, mounted at the top and the bottom of the aircraft fuselage, require (ideally) perfect 2π exposure of the complete hemisphere, which of course is not actually possible on the aircraft. For the upward looking sensor the only obstacles within the 2π field of view of the optical inlet are the propellers (about 2 m away) and one antenna (30 cm high and 10 cm wide, 50 cm away from the optical inlet), which, nevertheless do not seriously disturb the measurements. At aircraft roll angles of up to 6° (maximum possible angle adjustment range of the horizontal stabilization) some influence from the wings may affect the measurements, but this influence should be negligible too. The downward looking optical inlet is more or less unaffected, only the aircraft gear is within the field of view.

A sketch of the upward looking albedometer sensor is shown in Figure 6, a respective photo is depicted in Plate 1. Both give an idea of the practical realization of the active leveling mechanism and the connection between the 2-dimensional tilt stage and the quartz dome of the optical inlet system. An identical system is used for the downward looking component of the albedometer. The whole setup shown in Plate 1 has a weight of approximately 5 kg. It can easily be adopted to most aircraft.

4. MEASUREMENT EXAMPLES

To verify both, the horizontal stabilization and irradiance measurement performance, we have carried out an aircraft campaign near Dresden (Germany) with a small two-engined aircraft (Partenavia P68-B, D-GERY). The measurement site, the aircraft and its payload (beside the albedometer) are described by Keil et al. (2001). In the following we show and discuss downward irradiances measured under cloudless conditions carried out on 16 and 17 November 1999 (large solar zenith angle).

4.1. In-flight Performance Tests of the Horizontal Stabilization System

On 16 November 1999 we have performed several flights at constant altitude (about 3.300 m) in order to show the effects of the horizontal stabilization systems. During the horizontal flight legs the heading was changed from time to time and thus triangular and polygonal flight patterns were realized. Assuming no changes of the atmospheric conditions (in particular above the flight level), the measured downward irradiances should remain constant. To verify this, we have placed both optical inlet systems in the upward looking direction at the top of the aircraft. Thus both sensor heads were measuring downward radiation. Only one of both optical inlet systems was horizontally stabilized, while the second one was fixed at the aircraft fuselage. This second option is the usual sensor configuration in most atmospheric radiation research flights.

An example of the measurements is presented in Figure 7. The measured downward radiation (for a fixed wavelength of 633 nm) during a horizontal, polygonal flight pattern for both the horizontally stabilized and the fixed optical inlet are shown in Figure 7a (lower panel) as a function of time. In

Figure 7b (upper panel) the respective time series of the heading angle of the aircraft is plotted. Obviously, the measured irradiance level of the horizontally stabilized sensor remained constant at the different flight legs. Some slight decrease of the level is due to the decreasing sun elevation during the measurement period. During the sharp aircraft curves while changing the flight heading, the horizontal stabilization went out of range, which becomes obvious in the spikes of the measured irradiances during the flight curves. The spikes go into a positive or negative direction depending on the position of the tilted sensor during the curves with respect to the sun. Because the flight polygon was not closed (see Figure 7b), there was a difference between the measured irradiances at the beginning and at the end of the polygon.

However, compared to the horizontally stabilized optical inlet system the fixed sensor head reveals certain level jumps of the measured radiation between the different flight legs of the polygon. This is a typical feature for horizontal misalignment of the irradiance sensor. Again, the peaks in the measurements are obvious. At the end of the observation period, the difference between the measured data of the horizontally stabilized and the fixed sensor is in the order of 25%.

Beside the presented polygons, further triangular flight patterns (not shown) confirmed the performance of the horizontal stabilization system.

4.2. Spectral Downward Irradiances

To indicate the potential of the albedometer to measure spectral irradiances, we discuss an example from a descending flight pattern carried out on 17 November 1999.

In Figure 8 the vertical profiles of aerosol particle concentration and effective radius are presented, measured by an optical particle counter (Passive Cavity Aerosol Spectrometer Probe, PCASP-X, manufactured by PMS, Particle Measurement Systems, Boulder CO, USA). The PCASP-X counts and sizes single dry particles with diameters larger than 100 nm. Calibration and data analysis issues are described by Keil et al. (2001). A clear separation of the PBL (top around 1.500 m) and the free troposphere is obvious. This is confirmed by the vertical profiles of temperature and relative humidity (not shown), which prove the stable stratification of the atmosphere within the PBL during that flight. The size of the particles within the PBL is significantly larger than above the PBL, and the particle concentration steadily decreases with increasing altitude within the PBL.

The impact of these aerosol features on the measured downward spectral irradiances is shown in Figure 9. Within the PBL (thick, lower solid line) the spectral downward irradiances are significantly lower compared to the values measured above the PBL (thin, upper solid line). Also the spectral slope is lower within the PBL. The vertical error bars represent the effect of the 0.5° change of the solar zenith angle between the measurement of both spectra, which is estimated to be within $\pm 2-3\%$ from the graphs in Figure 1 (solar zenith angle of about 70°). The error bars show that the differences between the spectra is not caused by the change of sun position during the measurements. The decrease in radiation within the PBL is rather caused by the fact that more radiation is scattered back to the upper hemisphere due to more and larger aerosol particles within the PBL. The lower spectral slope is related to the larger particles within the PBL. Furthermore, the gas absorption bands of O_3 (≈ 580 nm), H_2O (about 595, 650, 695, 720, 790, 820, 900, & 940 nm), O_2 (687.2

& 689.3 nm; 760.8 & 763.8 nm) and even Fraunhofer lines are represented in the measured downward irradiances.

5. CONCLUSIONS AND OUTLOOK

We present a new albedometer for airborne spectral measurements (wavelength range between about 400 and 1000 nm) of up- and downward irradiances. Simple calculations show that in order to assure an accuracy of better than $\pm 1\%$ for the measured irradiances the horizontal misalignment of the sensor inlets must not exceed $\pm 0.2^\circ$ for solar zenith angles up to 70° . To realize this requirement a horizontal stabilization system was developed and tested in the laboratory and during real flights. Both have shown that the accuracy of the horizontal stabilization is better than the desired $\pm 0.2^\circ$ for both the aircraft pitch and roll angle for angular velocities up to 3°s^{-1} with a response time of the horizontal adjustment of 43 ms.

During a first aircraft campaign with the albedometer conducted near Dresden (Germany) in November 1999, the field suitability of the new instrument has been successfully demonstrated under cloudless conditions. Spectra of up- and downward irradiances have been recorded with a temporal resolution in the range of 1-5 s. One example of downward irradiance measurements above and within the PBL is presented. The difference between the spectra is clearly related to the enhanced aerosol particle concentrations and the resulting higher back-scattering of the incoming solar radiation within the PBL. In this way the potential of the new albedometer for radiation budget studies within the atmosphere is indicated.

In the future the albedometer will be used to perform spectral irradiance measurements in combination with meteorological, as well as microphysical

aerosol and cloud measurements, to pursue the study of the problem of enhanced absorption of solar radiation within both the cloudless and the cloudy sky. Combined with sophisticated radiative transfer calculations, the instrument offers the improved measurement accuracy and wavelength resolution necessary to reveal some of the reasons for the enhanced absorption problem. Furthermore, we plan to use the system to measure spectral actinic irradiances and derived photolysis frequencies by using isotropic (instead of cosine-weighting) optical inlet systems and a short-wavelength-optimized spectrometer system.

Acknowledgements: We are grateful to H. Franke and R. Maser from *enviscope* GmbH and S. Günnel from the electronic workshop of IfT for their help to install the albedometer on the aircraft. Furthermore, we thank our pilot, B. Schumacher from Rheinbraun AG, for his pleasant cooperation during the flights. E. von Hinüber from iMAR GmbH supported the setup of the horizontal stabilization system. J. Foot and A. Keil have carefully edited the manuscript.

REFERENCES

Asano, S., and Shiobara, M., 1989: Aircraft measurements of the radiative effects of tropospheric aerosols: I. Observational results of the radiation budget. *J. Meteor. Soc. Japan*, **67**, 847-861.

Asano, S., Shiobara, M., Nakanishi, Y., and Miyake, Y., 1995a: A multichannel cloud pyranometer system for airborne measurement of solar spectral reflectance by clouds. *J. Atmos. Oceanic Technol.*, **12**, 479-487.

Asano, S., Shiobara, M., and Uchiyama, A., 1995b: Estimation of cloud physical parameters from airborne solar spectral reflectance measurements for stratocumulus clouds. *J. Atmos. Sci.*, **52**, 3556-5376.

Bais, A. F., Kazadzis, S., Balis, D., Zerefos, C. S., and Blumthaler, M., 1998: Correcting global solar ultraviolet spectra recorded by a Brewer spectroradiometer for its angular response error. *Appl. Opt.*, **37**, 6339-6344.

Bannehr, L., and Glover, V., 1991: Preprocessing of airborne pyranometer data. *NCAR Tech. Note NCAR/TN-364+STR*, NCAR Inf. Serv., Boulder, CO, 35 pp.

Bannehr, L., and Schwiesow, R., 1993: A technique to account for the misalignment of pyranometers installed on aircraft. *J. Atmos. Oceanic Technol.*, **10**, 774-777.

Beaubien, D. J., Bisberg, A., and Beaubien, A. F., 1998: Investigations in pyranometer design. *J. Atmos. Oceanic Technol.*, **15**, 677-686.

Boers, R., Mitchell, R. M., and Krummel, P. B., 1998: Correction of aircraft pyranometer measurements for diffuse radiance and alignment errors. *J. Geophys. Res.*, **103**, 16753-16758.

Bush, B. C., Valero, F. P. J., Simpson, A. S., and Bignone, L., 2000: Characterization of thermal effects in pyranometers: A data correction algorithm for improved measurements of surface insulations. *J. Atmos. Oceanic Technol.*, **17**, 165-175.

Feister, U., Grewe, R., Gericke, K., 1997: A method for correction of cosine errors in measurements of spectral UV irradiances. *Sol. Energy*, **60**, 313-332.

Foot, J. S., Kitchen, M., and Readings, C. J., 1985: The measurement of diffuse solar radiation from an aircraft. *Atmos. Environ.*, **19**, 811-818.

Forgan, B. W., 1996: A new method for calibrating reference and field pyranometers. *J. Atmos. Oceanic Technol.*, **13**, 638-645.

Hagan, D., Crisp, D., Blavier, J.-F., DiGirolamo, L., and Ackerman, T., 1998: Balloon-based measurements of the profile of downwelling shortwave irradiance in the troposphere. *Geophys. Res. Lett.*, **25**, 1887-1890.

Harrison, L., Beauharnois, M., Berndt, J., Kiedron, P., Michalsky, J., and Min, Q., 1999: The rotating shadowband spectroradiometer (RSS) at SGP. *Geophys. Res. Lett.*, **26**, 1715-1718.

Halthore, R. N., and Schwartz, S. E., 2000: Comparison of model-estimated and measured diffuse downward irradiances at the surface in cloud-free skies. *J. Geophys. Res.*, **105**, 20165-20177.

Hayasaka, T., Kikuchi, N., and Tanaka, M., 1995: Absorption of solar radiation by stratocumulus clouds: Aircraft measurements and theoretical calculations. *J. Appl. Meteorol.*, **34**, 1047-1055.

Hignett, P., 1987: A study of the short-wave radiative properties of marine stratus: Aircraft measurements and model comparisons. *Quart. J. Roy. Met. Soc.*, **113**, 1011-1024.

Hignett, P., Taylor, J. P., Francis, P. N., and Glew, M. D., 1999: Comparison of observed and modeled direct aerosol forcing during TARFOX. *J. Geophys. Res.*, **104**, 2279-2287.

Hobbs, P. V., 1999: An overview of the University of Washington airborne measurements and results from Tropospheric Aerosol Radiative Forcing Observational Experiment (TARFOX). *J. Geophys. Res.*, **104**, 2233-2238.

Hofzumahaus, A., Kraus, A., and Müller, M., 1999: Solar actinic flux spectroradiometry: A technique for measuring photolysis frequencies in the atmosphere. *Appl. Opt.*, **38**, 4443-4460.

Keil, A., Wendisch, M., and Brüggemann, E., 2001: Measured profiles of aerosol particle absorption and its influence on clear-sky solar radiative forcing. *J. Geophys. Res.*, **106**, 1237-1247.

Kiedron, P. W., Michalsky, J. J., Berndt, J. L., and Harrison, L. C., 1999: Comparison of spectral irradiance standards used to calibrate shortwave radiometers and spectroradiometers. *Appl. Opt.*, **38**, 2432-2439.

Landelius, T., and Josefsson, W., 2000: Methods for cosine correction of broadband UV data and their effect on the relation between UV irradiance and cloudiness. *J. Geophys. Res.*, **105**, 4795-4802.

Meywerk, J., and Ramanathan, V., 1999: Observations of the spectral clear-sky aerosol forcing over the tropical Indian Ocean. *J. Geophys. Res.*, **104**, 24359-24370.

Michalsky, J., Dutton, E., Rubes, M., Nelson, D., Stoffel, T., Wesley, M., Splitt, M., and DeLuisi, J., 1999: Optimal measurement of surface shortwave irradiance using current instrumentation. *J. Atmos. Oceanic Technol.*, **16**, 55-69.

Oppitz, C., and Heering, W., 1998: Reflective optics for cosine-corrected irradiance measurements. *Rev. Sci. Instr.*, **69**, 3487-3490.

Ramaswamy, V., and Freidenreich, S. M., 1998: A high-spectral resolution study of the near-infrared solar flux disposition in clear and overcast atmospheres. *J. Geophys. Res.*, **103**, 23255-23273.

Russell, P. B., Livingston, J. M., Hignett, P., Kinne, S., Wong, J., Chien, A., Durkee, P., and Hobbs, P. V., 1999: Aerosol-induced radiative flux changes off the United States Mid-Atlantic coast: Comparison of values calculated from sunphotometer and in situ data with those measured by airborne pyranometer. *J. Geophys. Res.*, **104**, 2289-2307.

Saunders, R. W., Brogniez, G., Buriez, J. C., Meerkötter, R., and Wendling, P., 1992: A comparison of measured and modeled broadband fluxes from aircraft data during the ICE'89 field experiment. *J. Atmos. Oceanic Technol.*, **9**, 391-406.

Shetter, R. E., and M. Müller, 1999: Photolysis frequency measurements using actinic flux spectroradiometry during the PEM-tropics mission: Instrument description and some results. *J. Geophys. Res.*, **104**, 5647-5661.

Sicard, M., Thome, K. J., Crowther, B. G., and Smith, M. W., 1998: Shortwave infrared spectroradiometer for atmospheric transmittance measurements. *J. Atmos. Oceanic Technol.*, **15**, 174-183.

Stephens, G. L., 1996: How much solar radiation do clouds absorb?, *Science*, **271**, 1131-1133.

Taylor, J. P., 1994: Measurements of the radiative and microphysical properties of stratocumulus over the South Atlantic and around the British Isles. *Atmos. Res.*, **34**, 27-41.

Taylor, J. P., and McHaffie, A., 1994: Measurements of cloud susceptibility. *J. Atmos. Sci.*, **51**, 1298-1306.

Taylor, J. P., Edwards, J. M., Glew, M. D., Hignett, P., and Slingo, A., 1996: Studies with a flexible new radiation code. II: Comparisons with aircraft short-wave observations. *Q. J. R. Meteorol. Soc.*, **122**, 839-861.

Taylor, J. P., and Ackerman, A. S., 1999: A case-study of pronounced perturbations to cloud properties and boundary-layer dynamics due to aerosol emissions. *Q. J. R. Meteorol. Soc.*, **125**, 2643-2661.

Valero, F. P. J., Pope, S. K., Ellingson, R. G., Strawa, A. W., and Vitko Jr., J., 1996: Determination of clear-sky radiative flux profiles, heating rates and optical depths using unmanned aerospace vehicles as a platform. *J. Atmos. Oceanic Technol.*, **13**, 1024-1030.

Wendisch, M., and Keil, A., 1999: Discrepancy between measured and modeled solar and UV radiation within polluted boundary layer clouds. *J. Geophys. Res.*, **104**, 27373-27385.

Wendisch, M., Keil, A., Müller, D., Wandinger, U., Wendling, P., Stifter, A., Petzold, A., Fiebig, M., Wiegner, M., Freudenthaler, V., Armbruster, W., von Hoyningen-Huene, W., and Leiterer, U., 2001: Aerosol-radiation interaction in the cloudless atmosphere during LACE 98. Part 1: Measured and calculated solar and spectral surface insulations. Submitted to *J. Geophys. Res.*

TABLES

Table 1: Percentage deviation Φ_{ζ} [%] of the following radiation quantities ζ : irradiance F (Eqs. 2 and 3), layer's top albedo r , layer reflectance R , layer transmittance T , irradiance absorbed within the layer F_a , and layer's absorptance A for a horizontal misalignment of $\Delta\theta = 0.2^\circ$.

θ [°]	0	10	20	30	40	50	60	70	80
Φ_F [%]	-0.001	-0.062	-0.128	-0.202	-0.294	-0.417	-0.605	-0.960	-1.98
$\Phi_r = \Phi_R = \Phi_T$ [%]	0.001	0.062	0.128	0.203	0.294	0.418	0.609	0.969	2.02
Φ_{F_a} [%]	-0.004	-0.446	-0.916	-1.45	-2.11	-2.99	-4.34	-6.89	-14.2
Φ_A [%]	-0.004	-0.384	-0.789	-1.25	-1.82	-2.58	-3.76	-5.98	-12.5

Table 2: The same as Table 1, but for $\Delta\theta = 1.0^\circ$.

θ [°]	0	10	20	30	40	50	60	70	80
Φ_F [%]	-0.015	-0.323	-0.650	-1.02	-1.48	-2.10	-3.04	-4.81	-9.91
$\Phi_r = \Phi_R = \Phi_T$ [%]	0.015	0.324	0.655	1.03	1.50	2.14	3.13	5.05	11.0
Φ_{F_a} [%]	-0.109	-2.32	-4.67	-7.34	-10.6	-15.0	-21.8	-34.5	-71.1
Φ_A [%]	-0.094	-2.00	-4.04	-6.38	-9.27	-13.2	-19.3	-31.2	-67.9

FIGURE CAPTIONS

Figure 1: Percentage deviations of irradiance Φ_F as a function of horizontal misalignment $\Delta\theta$ for different values of solar zenith angle θ . The calculations are done using Eq. 2.

Figure 2: Percentage deviations of layer absorptance Φ_A as a function of horizontal misalignment $\Delta\theta$ for different values of solar zenith angle θ .

Figure 3: Scheme of the albedometer setup. The abbreviations are defined as follows: ACS: acceleration sensors, AHZ: artificial horizon, DAS: data acquisition system, GPS: global positioning system, 2DTS: 2-dimensional tilt stage, PC: personal computer, OI: optical inlet, and MCS: multi-channel spectrometer.

Figure 4: Time series of given (by the function generator) and measured (by the GPS-supported artificial horizon) roll angles (Figure 4a, lower panel), and of absolute difference between given and measured roll angles (Figure 4b, upper panel). Both given and measured angles are recorded with 10 Hz resolution; in the graph the measured angles are given with 1 Hz only. These results are obtained in laboratory tests using real aircraft attitude measurements to drive the function generator. The aircraft roll and pitch angle data were collected during a flight carried out on 16 November 1999 (descending pattern) in rather turbulent atmospheric conditions .

Figure 5: The same as Figure 4, but for the pitch angle.

Figures 6: Sketch of the 2-dimensional tilt stage together with the optical inlet for the upward looking albedometer sensor. A respective photo of both components is shown in Plate 1.

Figure 7: Time series of downward spectral irradiances (1 Hz resolution) at the wavelength of 633 nm (Figure 7a, lower panel) and of aircraft heading (Figure

7b, upper panel) measured during a flight near Dresden in about 3.300 m altitude on 16 November 1999. A horizontal polygonal flight pattern was performed. In Figure 7a the solid line represents the measurements with the horizontally stabilized sensor system, whereas the dashed line shows the data of the sensor head fixed at the aircraft fuselage. In Figure 7b the open circles show the time series of the aircraft heading.

Figure 8: Vertical profile of aerosol particle concentration and particle effective radius (1 Hz time resolution) measured near Dresden on a descending flight pattern on 17 November 1999. The planetary boundary layer (PBL) top height in about 1500 m altitude is indicated by a horizontal arrow.

Figure 9: Spectral downward irradiances above the PBL (13:01 UTC, solar zenith angle $\theta_s = 72.7^\circ$, solar azimuth angle $\varphi_s = 198^\circ$, 2.800 m altitude) and within the PBL (13:12 UTC, $\theta_s = 73.2^\circ$, solar azimuth angle $\varphi_s = 201^\circ$, 780 m altitude) and measured on the same flight as in Figure 8. The integration time for both spectra was 4 s. The vertical error bars indicate the estimated magnitude of $\pm 3\%$ uncertainty in the downward irradiances caused by the change of the solar zenith angle of 0.5° between the measurement of both spectra.

PLATE CAPTION

Plate 1: Photo of the 2-dimensional tilt stage together with the optical inlet for the upward looking albedometer sensor. A respective sketch of both components is shown in Figure 6.

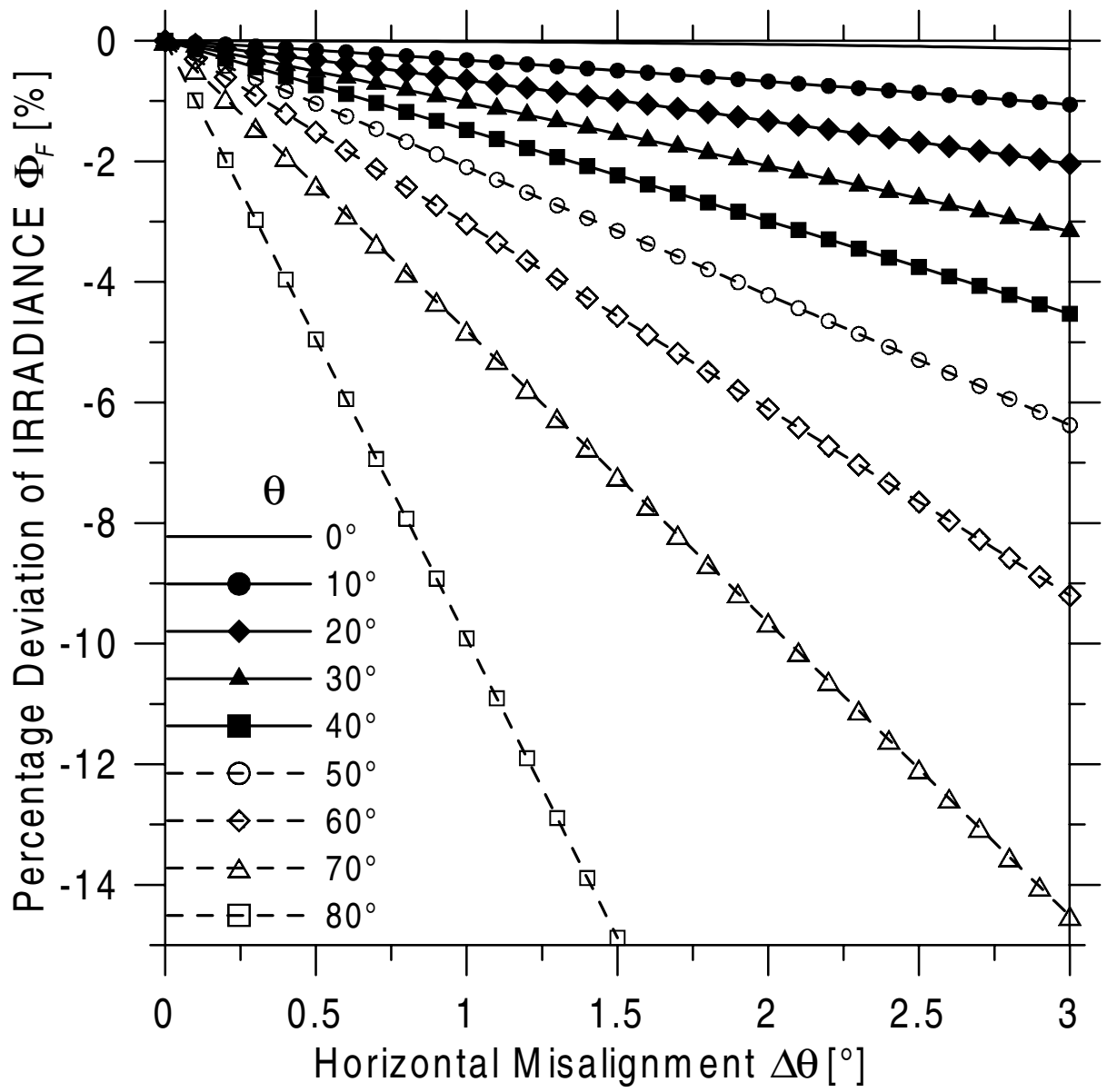


Figure 1

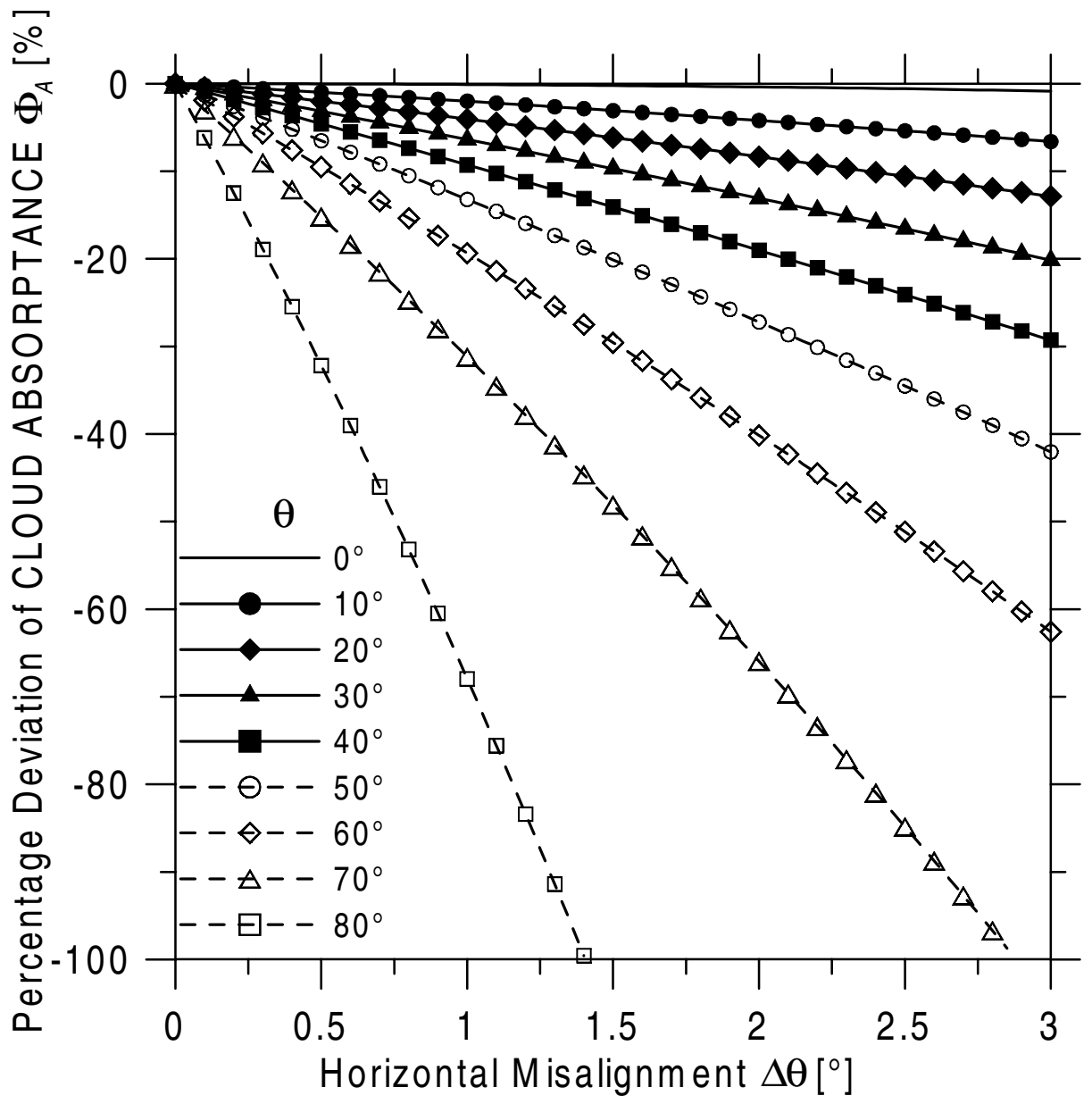


Figure 2

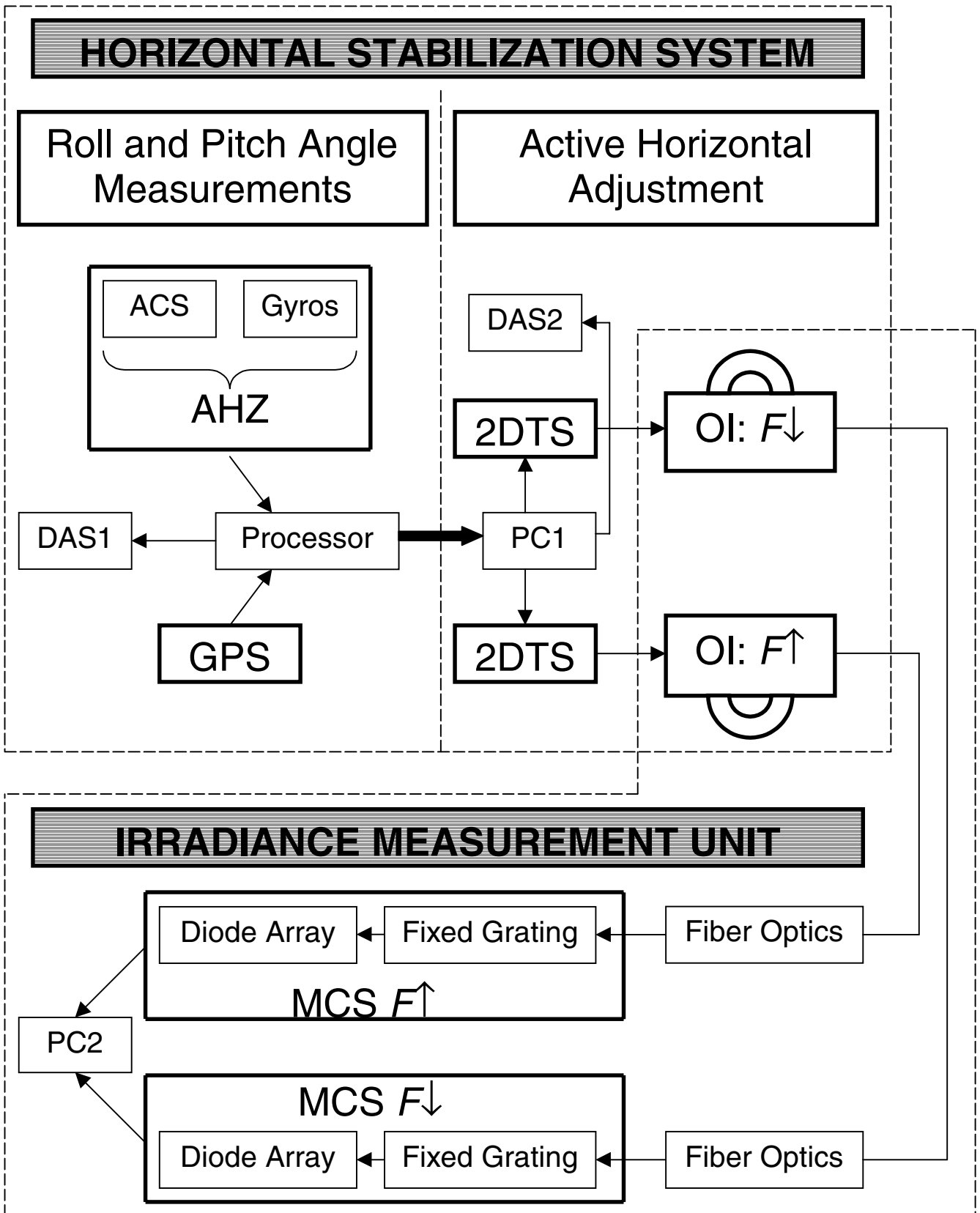


Figure 3

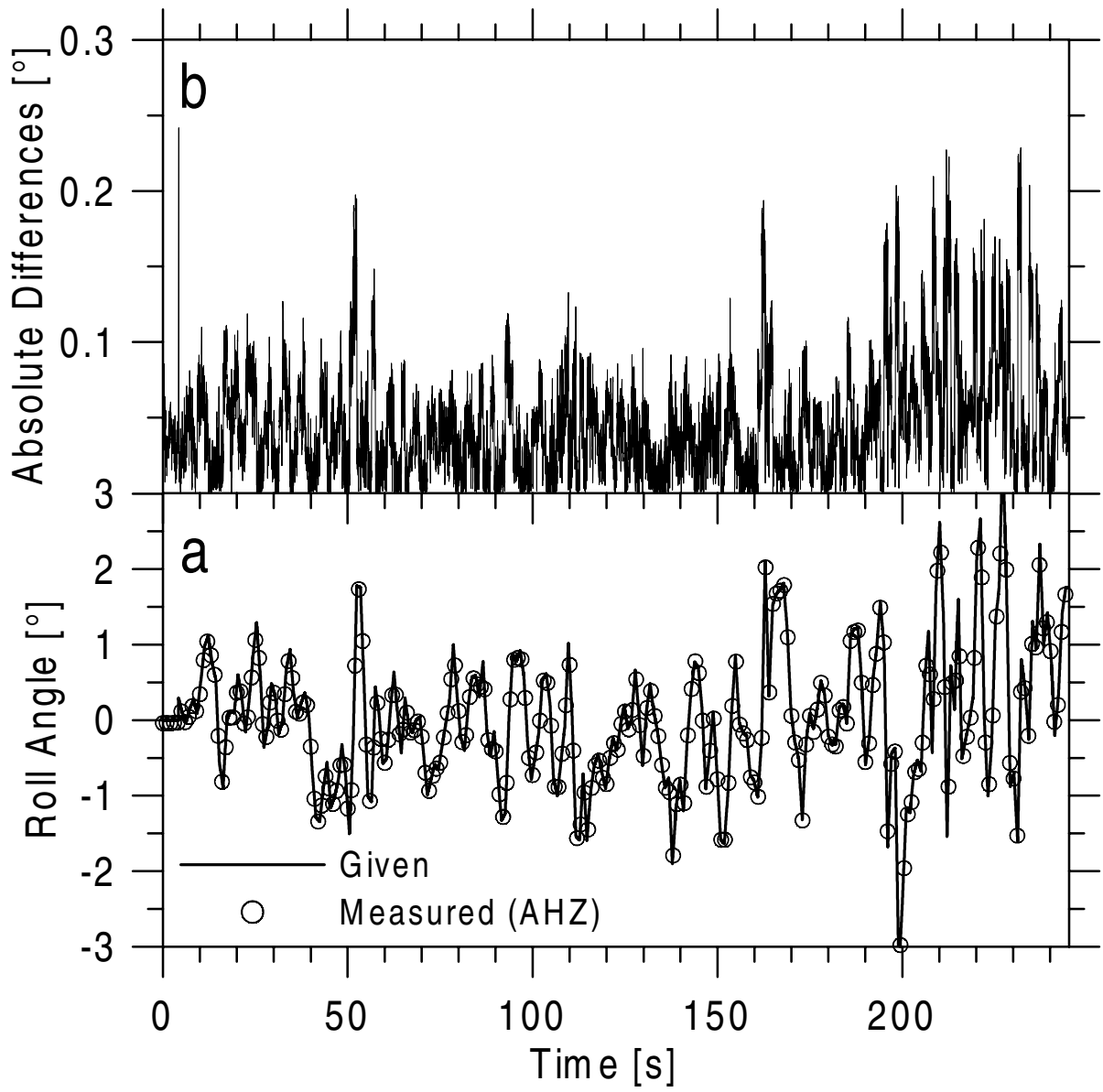


Figure 4

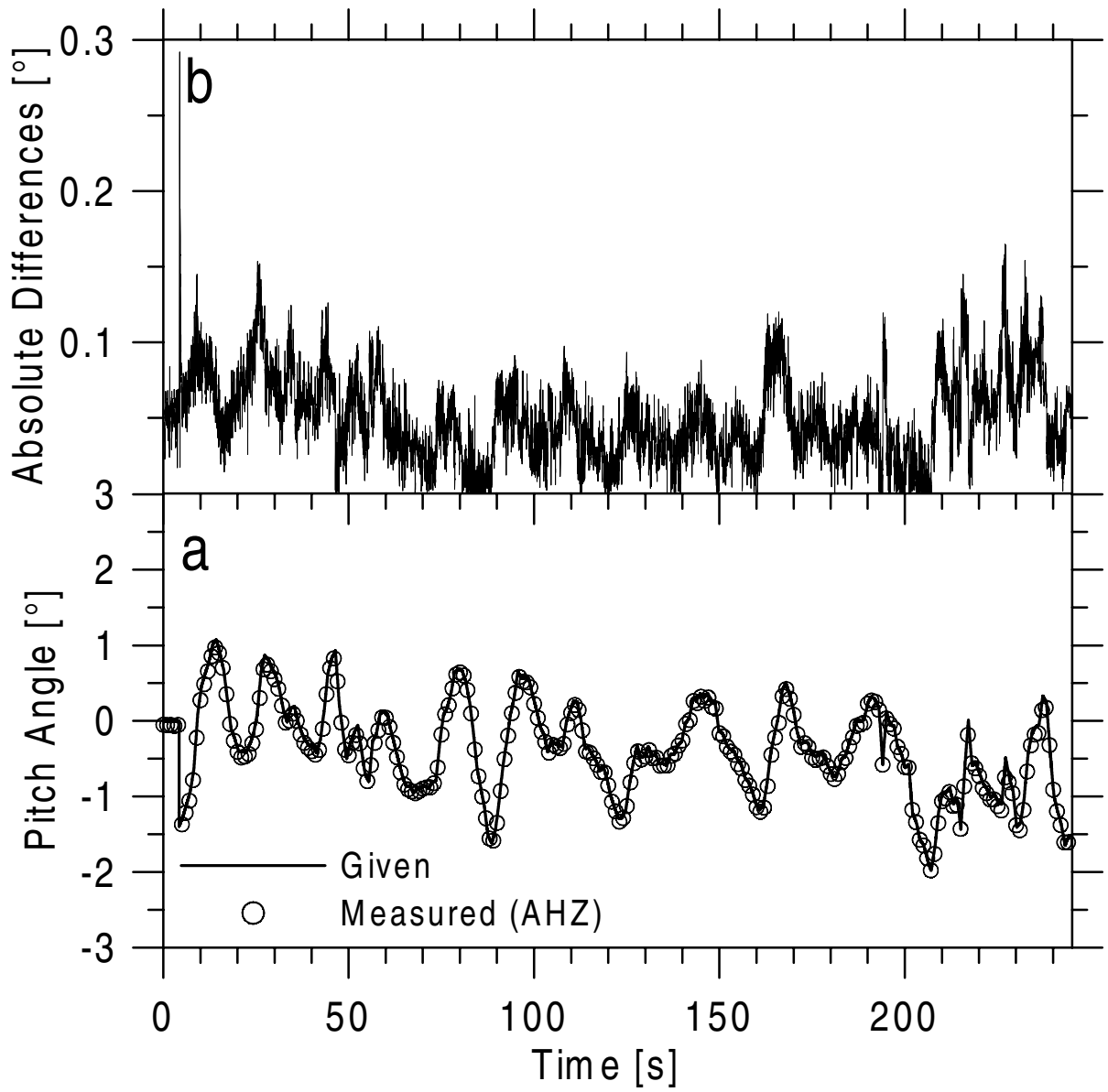


Figure 5

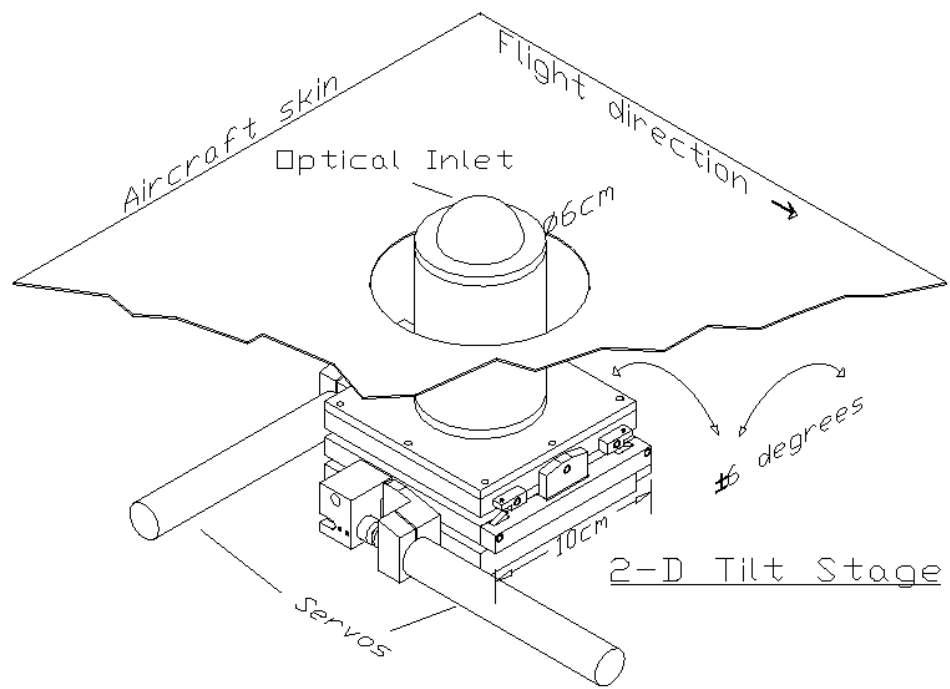


Figure 6

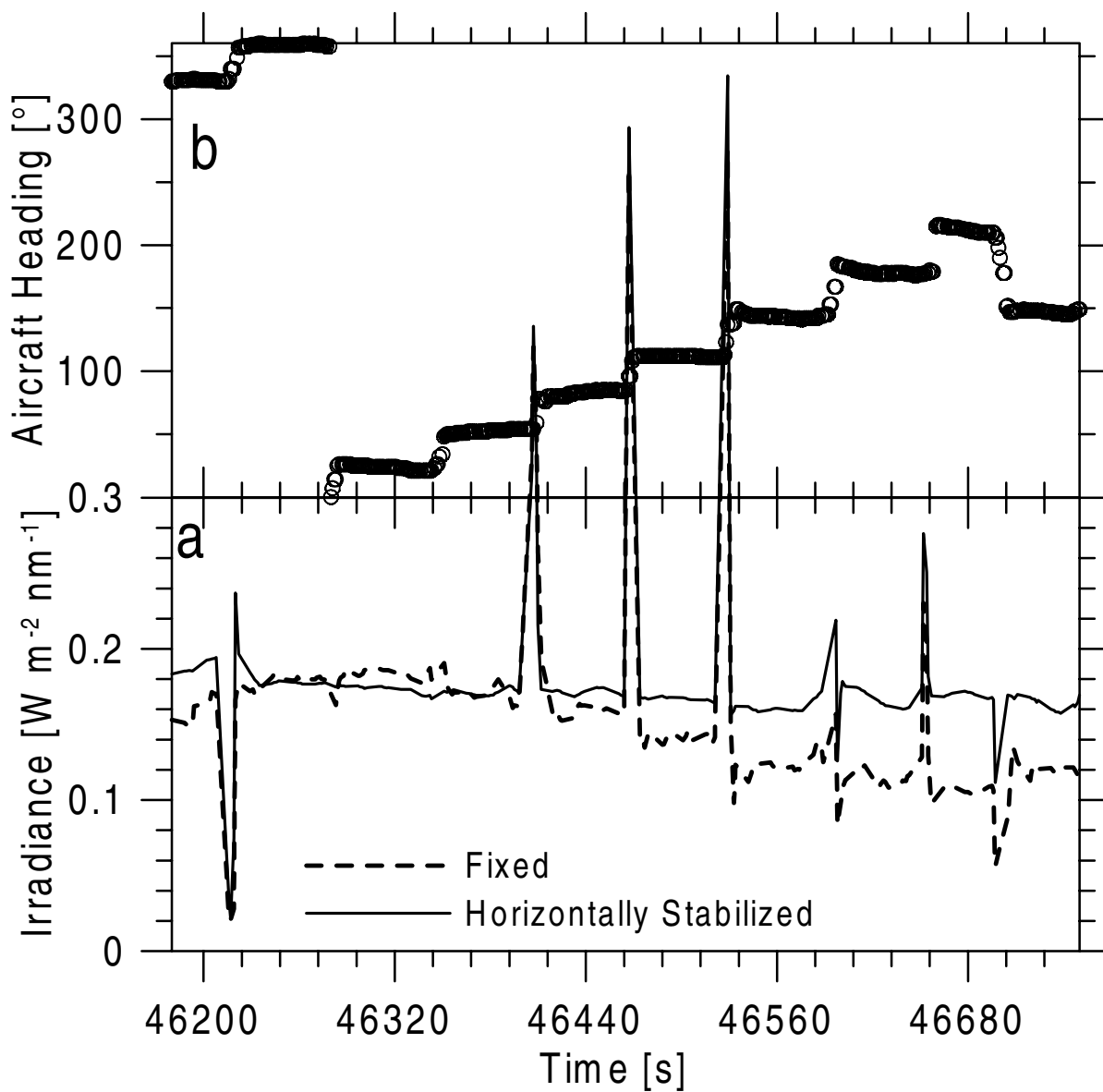


Figure 7

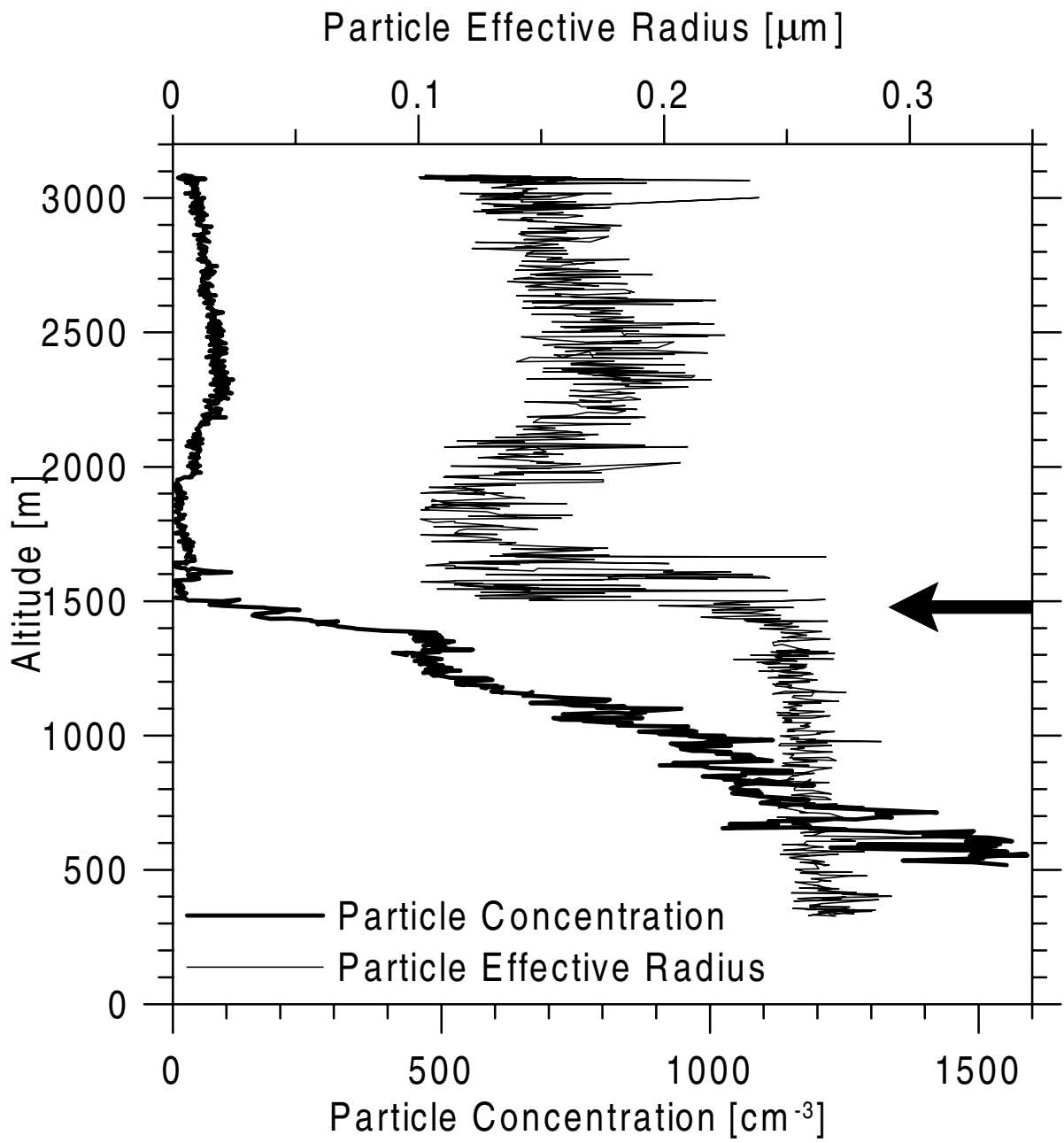


Figure 8

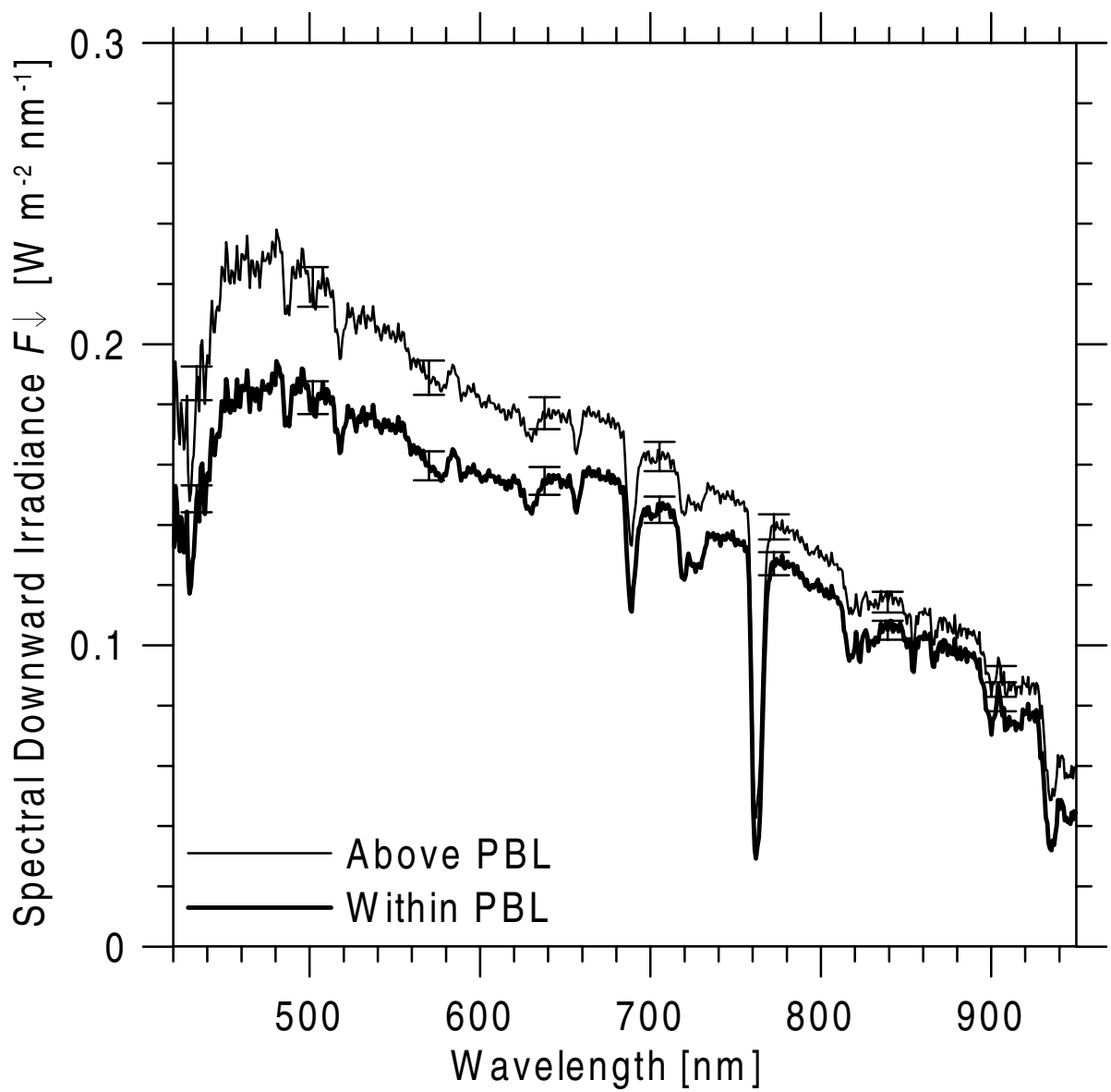


Figure 9

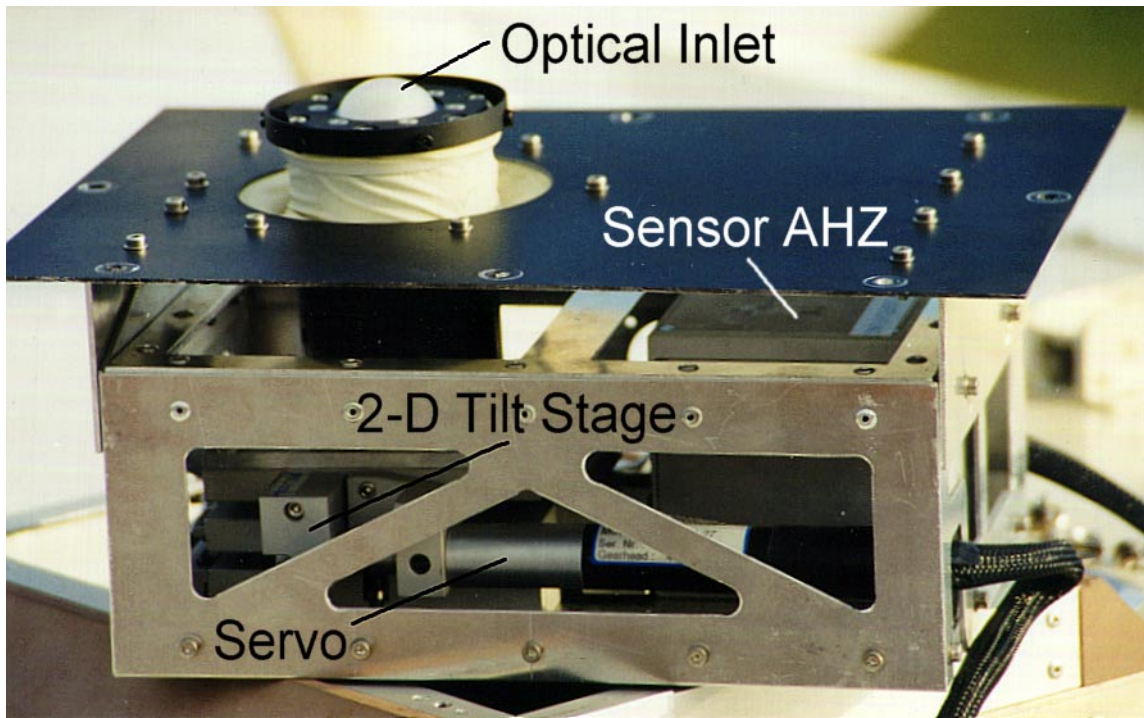


Plate 1